White-light interferometry on rough surfaces—measurement uncertainty caused by noise

Pavel Pavliček* and Ondřej Hýbl

Palacky University, Faculty of Science, Regional Centre of Advanced Technologies and Materials, Joint Laboratory of Optics of Palacky University and Institute of Physics of Academy of Science of the Czech Republic, Třida 17. listopadu 12, CZ-771 46 Olomouc, Czech Republic

*Corresponding author: Pavel.Pavlicek@upol.cz

Received 11 August 2011; revised 10 November 2011; accepted 10 November 2011; posted 15 November 2011 (Doc. ID 152706); published 26 January 2012

White-light interferometry on rough surfaces is an optical method for the measurement of the geometrical form of objects. The longitudinal coordinate of the measured surface is obtained from the measured interferogram by means of an evaluation method. However, the longitudinal coordinate cannot be determined completely accurately because the interferogram is affected by noise. We calculate the lower limit of the longitudinal measurement uncertainty caused by noise by use of the Cramer–Rao inequality. Additionally, we calculate the lower limit of the longitudinal measurement uncertainty caused by shot noise only. © 2012 Optical Society of America

OCIS codes: 030.4280, 100.2000, 120.3180.

1. Introduction

White-light interferometry is an established method to measure the geometrical form of objects. A typical setup for white-light interferometry is shown in Fig. 1. A Michelson interferometer is illuminated by a broadband light source such as a light-emitting diode, superluminescent diode, arc, or incandescent lamp. A CCD camera is used as a multiple detector at the output of the interferometer [1–5].

The measured object is placed in one arm of the interferometer and moved in the longitudinal direction while its surface is imaged by a suitable optical system onto the light-sensitive area of the CCD camera. The light reflected from the object is superimposed with the light from the reference arm. The intensity on the camera recorded as a function of the longitudinal coordinate z of the measured object is called the white-light interferogram [6]. An example of the white-light interferogram is presented in Fig. 2. The height profile of the measured object is acquired by the evaluation of the interferogram for each pixel of the CCD camera.

Originally, white-light interferometry was only used to measure the form of objects with optically smooth surfaces [1,2]. A surface is regarded as being optically smooth when its height variations within the resolution cell of the imaging system do not exceed one-eighth of the wavelength of the light used [7]. However, white-light interferometry can be used to measure the form of objects with rough surfaces as well, as was shown in [3,4]. A surface is regarded as being optically rough when its height variations within the resolution cell of the imaging system exceed one-fourth of the wavelength of the light used [7]. It follows that the property of being optically smooth or rough depends not only on the ratio of surface roughness to wavelength of used light but also on the size of the resolution cell of the imaging system [7–9]. When objects with optically rough surfaces are measured by white-light interferometry, a speckle pattern arises in the image plane [7, 10–12]. Therefore, white-light interferometry on rough

1559-128X/12/040465-09$15.00/0

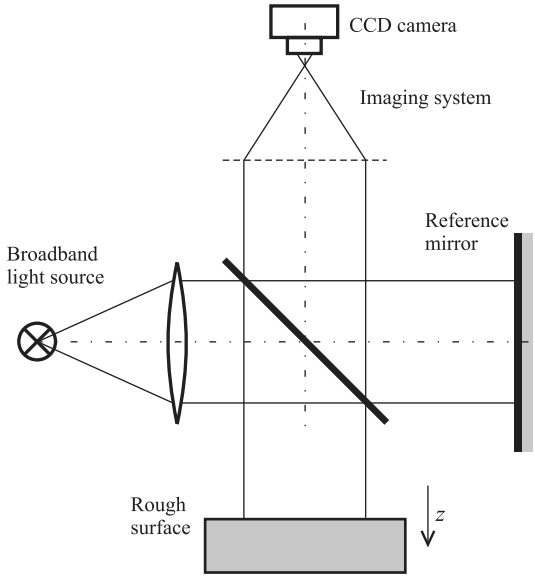

Fig. 1. Schematic of white-light interferometry.

surfaces does not resolve the lateral structure of the surface; it measures the overall geometrical form of the object.

When the surface of the measured object is optically smooth, the information about the height coordinate is obtained from both the phase and the envelope of the interferogram [1,2]. In white-light interferometry on optically rough surfaces, the phase of the white-light interferogram is not evaluated because it is a random variable [3,4,11,13]. The information about the height coordinate is obtained from the envelope of the interferogram only. The envelope of the interferogram is indicated with dashed line in Fig. 2. However, the measured interferogram is affected by the noise. Therefore, the height coordinate cannot be measured accurately; the noise is a source of measurement uncertainty. In this paper we deal with white-light interferometry on optically rough surfaces and discuss how the noise influences the measurement uncertainty.

The main sources of the noise in white-light interferometry on rough surfaces are the random arrival of photons at the detector (shot noise) [14], the variation of the moving speed of the object (positioning noise), and the discretization of analog signal (discretization noise) [15].

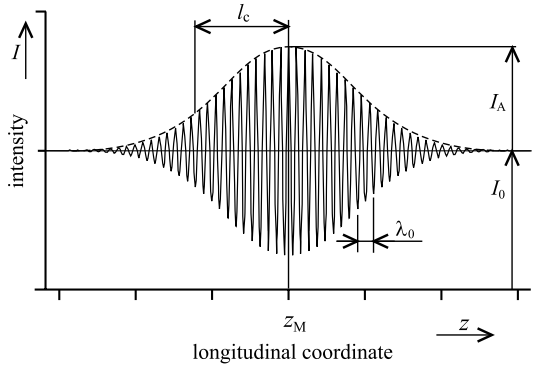

Fig. 2. White-light interferogram.

Fleischer *et. al.* developed a mathematical model for an ideal white-light interferometry evaluation algorithm affected by the noise [13]. They derived the lower limit of the longitudinal measurement uncertainty for both the phase and the envelope evaluation. Seiffert used the Cramer–Rao inequality for estimation of the longitudinal measurement uncertainty of white-light interferometry for the case of envelope evaluation [16]. In both studies [13,16], it is assumed that the standard deviation of the noise is constant over all samples.

Our goal here is to investigate the influence of noise on the measurement uncertainty. First, similar to [13,16], we assume that all samples are affected by a noise with a constant standard deviation. The calculation of the measurement uncertainty for white-light interferometry is performed in Section 4. For comparison, the measurement uncertainty of a sensor with signal without modulation is calculated in Section 5. The results obtained in Sections 4 and 5 are compared and discussed in Section 6.

The shot noise caused by the random arrival of photons at the detector holds a unique position among the noise sources mentioned above. As a fundamental property of the quantum nature of light, the shot noise cannot be, even theoretically, reduced. The shot noise imposes a basic limit on the minimum signal-to-noise ratio that can be achieved [14]. Therefore, we calculate additionally the measurement uncertainty of white-light interferometry for the case when the interferogram is affected by shot noise only in Section 7.

2. Model Signal and Noise

The interferogram is a set of N values of measured intensity $\{I_k\}$ recorded by the camera for N equidistant longitudinal positions $\{z_k\}$ of the measured object. The distance between two subsequent sampling positions is called sampling step Δz ($z_k = z_0 + k\Delta z$). From the point of view of information theory, the interferogram is a signal that consists of model signal m of a known type and noise n [17]:

$$I(z = z_k) = I_k = m_k + n_k, \qquad k = 0, 1, \ldots, (N-1). \tag{1}$$

For the usual light sources used in white-light interferometry, we can expect that the model signal has a form of a Gaussian curve modulated by a cosine function [13]:

$$m(z) = I_0 + I_A \exp\left[-\left(\frac{z - z_M}{l_c}\right)^2\right] \times \cos\left[\frac{4\pi}{\lambda_0}(z - z_M) + \varphi\right], \tag{2}$$

where I_0 is an offset, I_A is the amplitude of the modulation, z_M is the position of the maximum of the

interferogram's envelope, l_c is the coherence length according to the definition presented in [18], λ_0 is the central wavelength of the light source, and φ is a phase difference. The meaning of parameters I_0, I_A, z_M, l_c, and λ_0 is illustrated in Fig. 2.

By comparing Eq. (2) with the interference law, the offset can be expressed by means of the amplitude I_A of modulation and the intensity I_R in the reference arm [18]. Equation (2) takes the form

$$m(z) = I_R + \frac{I_A^2}{4I_R} + I_A \exp\left[-\left(\frac{z - z_M}{l_c}\right)^2\right] \times \cos\left[\frac{4\pi}{\lambda_0}(z - z_M) + \varphi\right]. \quad (3)$$

As intensity I_R, coherence length l_c, wavelength λ_0, and phase difference φ are constant, the model signal depends on two parameters I_A and z_M.

For an uncorrelated noise with a normal distribution and a signal-independent standard deviation σ, the joint probability density function $p(I_k, a_i)$ of the measured signal I_k and the parameters a_i has the form [17]

$$p(I_k, a_i) = \left(\frac{1}{2\pi\sigma^2}\right)^{\frac{N}{2}} \exp\left[-\frac{1}{2\sigma^2}\sum_{k=0}^{N-1}(I_k - m_k)^2\right], \quad (4)$$

with $i = 1, \ldots, N_p$, where N_p is the number of parameters.

3. Cramer–Rao Inequality

The Cramer–Rao inequality, also referred to as the Cramer–Rao lower bound, defines the theoretical lower limit on the variance of an estimator of a parameter of a distribution [19]. In our case, the distribution is the set of measured intensities $\{I_k\}$ that we call interferogram, and the parameter of interest is the position of the maximum of the interferogram's envelope that means the longitudinal coordinate of the measured surface. The estimator is the algorithm that is used to find the maximum of the interferogram's envelope. Thus, the Cramer–Rao inequality defines the theoretical lower limit on the variance of the longitudinal coordinate of the measured surface. Finally, the variance of the longitudinal coordinate of the measured surface is the square of the longitudinal measurement uncertainty.

The lower limit of the variance $\sigma_{a_i}^2$ of a parameter a_i is given by the Cramer–Rao inequality. For a nonbiased estimator, the Cramer–Rao inequality has the form

$$\sigma_{a_i}^2 \geq (J^{-1})_{ii}, \quad (5)$$

where $(J^{-1})_{ii}$ is the ith diagonal element (the element with indices ii) of the inverse Fisher information matrix [17]. An estimator is called nonbiased if its expectation value is equal to the true value and is called efficient if the two sides of Eq. (5) are equal [19,20]. The Fisher information matrix is a $N_p \times N_p$ matrix with elements given by

$$J_{ij} = -\mathrm{E}\left[\frac{\partial^2 \ln p}{\partial a_i \partial a_j}\right], \quad (6)$$

where p is the joint probability density function and $E[]$ denotes the expected value related to the distribution.

In what follows, we will apply the Cramer–Rao inequality on the interferogram and will find the limit of the longitudinal measurement uncertainty. According to Eqs. (6) and (4), the elements of the Fisher information matrix are given by

$$J_{ij} = \frac{1}{\sigma^2}\sum_{k=0}^{N-1}\left(\frac{\partial m_k}{\partial a_i}\frac{\partial m_k}{\partial a_j}\right). \quad (7)$$

For practical computation of the parameters, the least-squares method can be used. If the noise is independent on the signal and normally distributed, the least-squares method is identical to the maximum likelihood estimator. Therefore, the least-squares method is an unbiased and efficient estimator for a normally distributed noise and a model signal that is linear in its parameters. In our case, the condition of normally distributed noise is satisfied [Eq. (4)] but the model signal is not linear in its parameters [Eq. (2)]. The nonlinearity implies that the least-squared method becomes a biased estimator. Nevertheless, the least-squares method can be considered as a nonbiased and efficient estimator when the standard deviation σ of the noise is small in comparison with the amplitude of modulation I_A [20].

4. Measurement Uncertainty of White-Light Interferometry on Rough Surfaces

The model signal of white-light interferometry is described by Eq. (2) and shown in Fig. 2. For the modulated signal, we assume that $I_A \leq I_0$ as follows from Eq. (3). Phase difference φ is for the case of optically rough surfaces a random number with a uniform distribution on the interval $[0, 2\pi)$ [21]. Thus, Eq. (2) can be rewritten in the form

$$m(z) = I_0 + I_A \exp\left[-\left(\frac{z - z_M}{l_c}\right)^2\right]\cos\left(\frac{4\pi}{\lambda_0}z + \varphi_1\right), \quad (8)$$

where φ_1 is also a random number with a uniform distribution on the interval $[0, 2\pi)$. Note that φ_1 is random but constant over all samples $(k = 0, \ldots, N - 1)$.

The model signal described by Eq. (8) has two parameters ($N_p = 2$):$a_1 = I_A$ and $a_2 = z_M$. The Fisher information matrix is a 2×2 matrix, and its elements are calculated using Eq. (7):

$$J_{11} = \frac{1}{\sigma^2}\sum_{k=0}^{N-1}\left\{\exp\left[-2\left(\frac{z_k - z_M}{l_c}\right)^2\right]\cos^2\left(\frac{4\pi}{\lambda_0}z_k + \varphi_1\right)\right\}, \tag{9}$$

$$J_{22} = \frac{4I_A^2}{\sigma^2 l_c^4}\sum_{k=0}^{N-1}\left\{\exp\left[-2\left(\frac{z_k - z_M}{l_c}\right)^2\right](z_k - z_M)^2 \times \cos^2\left(\frac{4\pi}{\lambda_0}z_k + \varphi_1\right)\right\}, \tag{10}$$

$$J_{12} = J_{21} = \frac{2I_A}{\sigma^2 l_c^2}\sum_{k=0}^{N-1}\left\{\exp\left[-2\left(\frac{z_k - z_M}{l_c}\right)^2\right](z_k - z_M) \times \cos^2\left(\frac{4\pi}{\lambda_0}z_k + \varphi_1\right)\right\} = 0. \tag{11}$$

The cosine function in Eq. (8) is treated as a constant in the differentiation with respect to z_M. This reflects the fact that the phase of the interferogram is not evaluated when measuring on the optically rough surfaces. The summed function in Eq. (11) is an odd function with respect to $z_k - z_M$. Therefore, the nondiagonal elements of J are equal to zero, and the Fisher information matrix is a diagonal matrix. The diagonal elements of the inverse Fisher information matrix can easily be expressed:

$$(J^{-1})_{ii} = (J_{ii})^{-1}. \tag{12}$$

From the Cramer–Rao inequality [Eq. (5)], we obtain the lower limit of the variance of position z_M:

$$\sigma_{z_M}^2 \geq J_{22}^{-1}. \tag{13}$$

Equation (10) can be further simplified. In practice, the interferogram is evaluated in a certain evaluation interval about the sought value z_M. We denote by J'_{22} the diagonal element of the Fisher information matrix calculated from the values corresponding to the evaluation interval:

$$J'_{22} = \frac{4I_A^2}{\sigma^2 l_c^4}\sum_{k=s-n}^{s+n}\left\{\exp\left[-2\left(\frac{z_k - z_M}{l_c}\right)^2\right](z_k - z_M)^2 \times \cos^2\left(\frac{4\pi}{\lambda_0}z_k + \varphi_1\right)\right\}. \tag{14}$$

Only n values of the interferogram on each side of the center $z_S = s\Delta z$ of the evaluation interval are entered into the sum. It would be ideal to set $z_S = z_M$. However, the position z_M is not known in advance. Therefore, in practice, the position z_S is found as a first approximation by a maximum searching method. Subsequently, the sought value z_M is determined by the accurate evaluation of the interferogram. Anyway, we can assume that the center z_S of the evaluation interval is located in the vicinity of the sought value z_M.

The discrete sum in Eq. (14) can be replaced by integral

$$\sum_{k=s-n}^{s+n}\left\{\exp\left[-2\left(\frac{z_k - z_M}{l_c}\right)^2\right](z_k - z_M)^2\cos^2\left(\frac{4\pi}{\lambda_0}z_k + \varphi_1\right)\right\} \cong \frac{1}{\Delta z}\int_{-L}^{L}\exp\left[-2\left(\frac{z}{l_c}\right)^2\right]z^2\cos^2\left(4\pi\frac{z}{\lambda_0} + \varphi\right)\mathrm{d}z. \tag{15}$$

Radius L of the integration interval is given by $L = n\Delta z$. The integral in Eq. (15) can be evaluated [22]. The modified element J'_{22} of the Fisher information matrix is then equal to

$$J'_{22} \cong \frac{1}{2}\sqrt{\frac{\pi}{2}}\frac{I_A^2}{\sigma^2}\frac{1}{l_c\Delta z}\left[\mathrm{erf}\left(\sqrt{2}u\right) - 2\sqrt{\frac{2}{\pi}}u\exp(-2u^2)\right], \tag{16}$$

where erf( ) is the error function and u denotes the ratio $u = L/l_c$ [19]. By inserting the result of Eq. (16) into Eq. (13), we obtain the lower limit of the measurement uncertainty

$$\delta z = \sigma_{z_M} \geq C\sqrt{2}\sqrt[4]{\frac{2}{\pi}}\frac{\sigma}{I_A}\sqrt{\Delta z l_c}, \tag{17}$$

where C is a constant brought about by the evaluation of the interferogram in a limited interval:

$$C = \left[\mathrm{erf}\left(\sqrt{2}u\right) - 2\sqrt{\frac{2}{\pi}}u\exp(-2u^2)\right]^{-1/2}. \tag{18}$$

Evidently it holds $C \geq 1$. For $L \gtrsim \sqrt{2}\,l_c$ ($u \gtrsim \sqrt{2}$), the constant C is approximately equal to 1. This corresponds to an ideal evaluation where all points of the interferogram are exploited. For the ideal evaluation, Eq. (17) goes over to

$$\delta z \geq \sqrt{2}\sqrt[4]{\frac{2}{\pi}}\frac{\sigma}{I_A}\sqrt{\Delta z l_c}. \tag{19}$$

5. Measurement Uncertainty of a Sensor with Signal without Modulation

A signal without modulation appears, e.g., in the confocal microscope or in shape from focus sensor [23–28]. The model signal is described by

$$m(z) = I_0 + I_A\exp\left[-\left(\frac{z - z_M}{l_c}\right)^2\right]. \tag{20}$$

The signal without modulation according to Eq. (20) is shown in Fig. 3. The ratio of intensities I_A and I_0 may be arbitrary. Evidently, the quantities I_A and l_c have here not the meaning of the amplitude of modulation and coherence length, respectively, but they can be considered as measures describing the form of

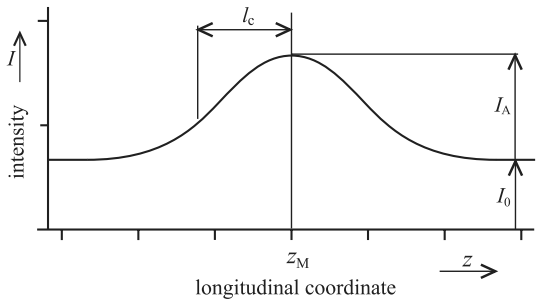

Fig. 3. Signal without modulation.

the signal. The signal without modulation described by Eq. (20) has the same two parameters: $a_1 = I_A$ and $a_2 = z_M$ as the signal with modulation described by Eq. (2).

Using the same mathematical procedure as in Section 4, we obtain for the measurement uncertainty

$$\delta z = \sigma_{z_M} \geq C \sqrt[4]{\frac{2}{\pi}} \frac{\sigma}{I_A} \sqrt{\Delta z l_c}. \tag{21}$$

The constant C is defined in Eq. (18). For the ideal evaluation, Eq. (21) goes over to

$$\delta z \geq \sqrt[4]{\frac{2}{\pi}} \frac{\sigma}{I_A} \sqrt{\Delta z l_c}. \tag{22}$$

6. Discussion

One can see from Eqs. (19) and (22) that measurement uncertainty δz depends in both cases proportional on the square root $\sqrt{l_c \Delta z}$ and the noise-to-signal ratio σ / I_A. In the case of the signal with modulation (white-light interferometry), the measurement uncertainty δz is by the factor $\sqrt{2}$ higher than that in the case of the signal without modulation. If the noise is determined (analytically or experimentally), the measurement uncertainty can be calculated.

The result described by Eq. (22) can be compared with the results obtained by Seiffert [16] and Fleischer [13]. However, one must take into account that the coherence length is defined in a different way in the cited works: $l_c(\text{Seiffert}) = 2^{3/2} l_c$ and $l_c(\text{Fleischer}) = 4\sqrt{\ln 2}\, l_c$. The comparison shows that the result given by Eq. (22) is the same as the result of Seiffert and by factor $\sqrt{2}$ higher than the result of Fleischer given by Eq. (37) in [13]. The difference between the results given by Eqs. (22) and Eq. (37) in [13] is caused by an incorrect evaluation of the integral in Eq. (37) in [13]. Nevertheless, the dependence of the measurement uncertainty on the coherence length, the sampling step, and noise-to-signal ratio is of the same form as that described in [13,16].

Fleischer shows that the demodulated signal has the same signal-to-noise ratio as the original signal [13]. From this fact, both Fleischer and Seiffert conclude that the measurement uncertainty in the case of signal with modulation is the same as that in the case of the signal without modulation. But the same signal-to-noise ratio is not a sufficient condition for the same measurement uncertainty. The noise of the demodulated signal can indeed have the same standard deviation as the noise of the original signal; however, it is no more uncorrelated.

The correlation of the noise of the demodulated signal is obvious from Fig. 4. Figure 4(a) shows a simulation of a signal with normally distributed uncorrelated noise and its envelope (signal after demodulation) evaluated by means of Hilbert transform [29]. The noise of the demodulated signal is compared with the noise of the original signal in Fig. 4(b). It is apparent that, while the noise of the original signal is an uncorrelated white noise, the noise of the demodulated signal is correlated. The correlation of the noise of the demodulated signal is also apparent from the comparison of the respective correlation functions in Fig. 4(c). The correlation function $R(k)$ of the noise is calculated according to [30]

$$R(k) = \frac{1}{(N-k)\sigma^2} \sum_{t=0}^{N-k-1} n_t n_{t+k}. \tag{23}$$

Because the noise of the demodulated signal is not uncorrelated, the condition for the validity of Eq. (4) is not satisfied.

The statement that the noise of the demodulated signal has the same standard deviation as the noise of the original signal is not generally valid. Demodulation by means of Hilbert transform is a typical example of demodulation algorithm where the noise of the demodulated signal has the same standard deviation as the noise of the original signal. However,

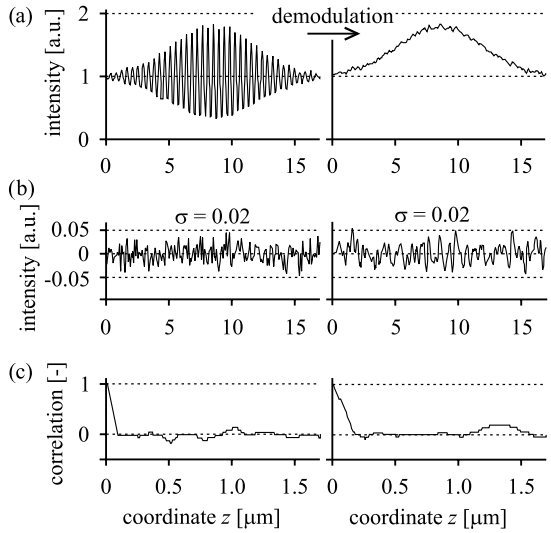

Fig. 4. Demodulation of a simulated interferogram by means of Hilbert transform ($\Delta z = \lambda_0/10$). (a) Signal before and after the demodulation. (b) Noise extracted from the signal. (c) Correlation function of the noise.

one can find demodulation algorithms for which the noise of the demodulated signal has even a lower standard deviation than the noise of the original signal. As an example of such an algorithm, we can mention the five-step phase-shifting algorithm described in [6]

$$4M^2\sin^4\psi = (I_2 - I_4)^2 - (I_1 - I_3)(I_3 - I_5), \qquad (24)$$

where M is the sought amplitude of modulation, ψ is the phase step between two consecutive samples, and I_i are the samples with $i = 1, 2, \ldots, 5$.

A simulation of a signal with normally distributed uncorrelated noise and the signal demodulated by means of the five-step phase-shifting algorithm described by Eq. (24) is shown in Fig. 5(a) for $\psi = 72^\circ$. The noise of the demodulated signal is compared with the (uncorrelated white) noise of the original signal in Fig. 5(b). It is apparent that the standard deviation of the noise of the demodulated signal is lower than that of the original signal. Also, it is apparent that the correlation of the noise of the demodulated signal is higher than that of the original signal. The correlation of the noise of the demodulated signal is in this case higher than that of the demodulated signal shown in Fig. 4. The correlation function of the noise of the demodulated signal is compared with the correlation function of the noise of the original signal in Fig. 5(c).

The minimal achievable measurement uncertainty has in the case of both examples (Hilbert transform, five-step phase-shifting algorithm) the same value given by Eq. (19). The two examples show that the value of the noise-to-signal ratio of the demodulated envelope is not significant. Whether it is the same as in the original signal (e.g., Hilbert transform) or is even lower (five-step phase-shifting algorithm), the minimal achievable measurement uncertainty is given by Eq. (19).

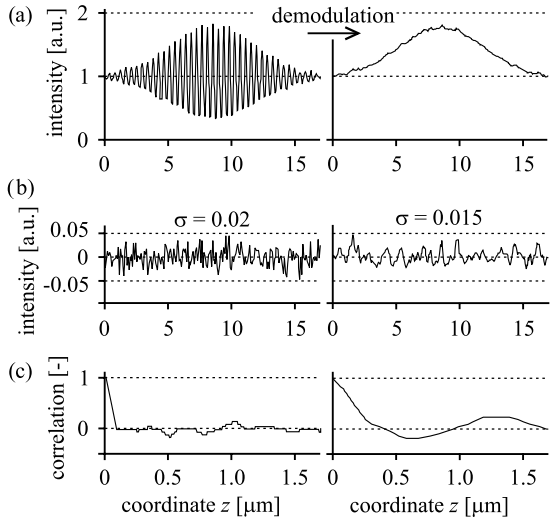

Fig. 5. Demodulation of a simulated interferogram by means of five-step phase-shifting algorithm ($\Delta z = \lambda_0/10$). (a) Signal before and after the demodulation. (b) Noise extracted from the signal. (c) Correlation function of the noise.

For the case of a correlated noise, Eq. (4) must be replaced by a more general relation [30]

$$p(I_k, a_i) = \left(\frac{1}{2\pi\sigma^2}\right)^{\frac{N}{2}} \times \exp\left\{-\frac{1}{2\sigma^2}\sum_{k=0}^{N-1}\sum_{l=0}^{N-1}[(I_k - m_k)r_{kl}(I_l - m_l)]\right\}, \qquad (25)$$

where r_{kl} are the elements of the reciprocal correlation matrix. The correlation matrix is a symmetric matrix obtained from the correlation function [19]. Examples of the correlation function of the noise are shown in the right side of Fig. 4(c) for the signal demodulated by means of Hilbert transform and in the right side of Fig. 5(c) for the signal demodulated by means of the five-step phase-shifting algorithm described by Eq. (24).

The elements of the Fisher information matrix for the case of the correlated noise are given by

$$J_{ij} = \frac{1}{\sigma^2}\sum_{k=0}^{N-1}\sum_{l=0}^{N-1}\left(\frac{\partial m_k}{\partial a_i} r_{kl} \frac{\partial m_l}{\partial a_j}\right). \qquad (26)$$

The element J_{22} of the Fisher information matrix is for the model signal described by Eq. (20) equal to

$$J_{22} = \frac{4I_A^2}{\sigma^2 l_c^4}\sum_{k=0}^{N-1}\sum_{l=0}^{N-1}\left\{\exp\left[-\left(\frac{z_k - z_M}{l_c}\right)^2\right](z_k - z_M)r_{kl} \times \exp\left[-\left(\frac{z_l - z_M}{l_c}\right)^2\right](z_l - z_M)\right\}. \qquad (27)$$

Equation (27) represents a generalization of Eq. (10) for the correlated noise. Note that the correlation matrix and its reciprocal become identity matrices for the case of uncorrelated noise, and Eq. (27) goes over into Eq. (10).

The element J_{22} can be calculated numerically according to Eq. (27). The numerical calculations show that the element J_{22} for the case of the signal with modulation is equal to the half of the element J_{22} for the case of the signal without modulation. The ratio 1/2 between J_{22} for the signal with modulation and J_{22} for the signal without modulation is independent on coherence length l_c, wavelength λ_0, and sampling step Δz.

For the nondiagonal elements it holds $J_{12} = J_{21} = 0$ also in the case of the signal with modulation. Thus, according to Eqs. (12) and (13), measurement uncertainty δz is in the case of the signal with modulation by factor $\sqrt{2}$ higher than in the case of the signal without modulation. This is in agreement with the result shown in Section 4.

7. Measurement Uncertainty of White-Light Interferometry on Rough Surfaces Caused by Shot Noise

The result described by Eq. (19) can be used for the determination of the lower limit of measurement uncertainty caused by shot noise. As was mentioned in Section 1, the shot noise of the camera is the component of the noise that cannot be reduced.

In white-light interferometry, light sources with a short coherence length are used. The light of these sources is classified as a chaotic light with several independent degrees of freedom. Such a light obeys the Mandel–Rice photocount distribution. However, when the integration time of the camera is much higher than the coherence time of the used light, the number of the independent degrees of freedom is large and the photocount distribution turns into Poisson distribution [31]. It holds for the Poisson distribution that the variance $(\Delta n_p)^2$ of photocounts is equal to the number n_p of photocounts

$$(\Delta n_p)^2 = n_p. \tag{28}$$

For large n_p, Poisson distribution can be approximated by normal distribution with mean n_p and variance n_p [14].

The intensity I measured by a camera with digital output is expressed in units of DN, where DN stands for "digital number" and means one step of the analog-to-digital (AD) converter. The ratio between the impinging optical energy and the measured intensity I is described by sensitivity H of the camera. The measured intensity I is proportional to the number n_p of photocounts

$$I = I_M \frac{n_p}{n_{\mathrm{FW}}}, \tag{29}$$

where n_{FW} is the maximal number of photocounts that can be collected by one pixel of the camera (full-well capacity) and I_M is the measured intensity corresponding to n_{FW}. An example of the signal is shown in Fig. 6. Intensity I_M is indicated with a dashed line.

The variance $(\Delta I)^2$ of the measured intensity I describes the shot noise of the camera. It follows from Eqs. (28) and (29)

$$\sigma = \Delta I = \sqrt{\frac{I_M}{n_{FW}} I}, \tag{30}$$

which means that the standard deviation σ of the noise is proportional to the square root of the measured intensity I. According to Eqs. (30), (1), and (2), the standard deviation σ of the noise is different in each point of the interferogram. However, a mean standard deviation $\bar{\sigma}$ of the noise can be introduced:

$$\bar{\sigma}^2 = \frac{1}{N}\sum_{k=0}^{N-1} \sigma_k^2 = \frac{1}{N}\frac{I_M}{n_{\mathrm{FW}}}\sum_{k=0}^{N-1} I_k. \tag{31}$$

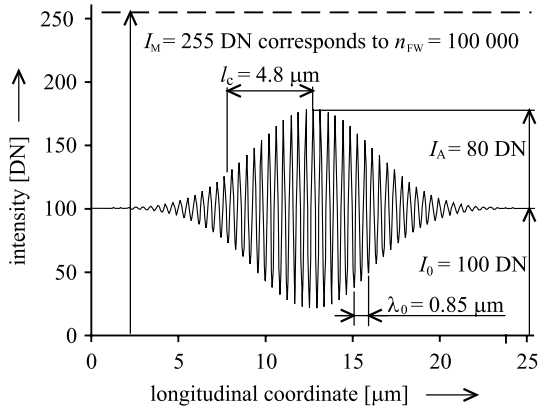

Fig. 6. Example of a model interferogram: $\lambda_0 = 850\,nm$, FWHM $= 40nm$, $I_M = 255$ DN, $I_0 = 100$ DN, and $I_A = 80$ DN.

The mean standard deviation is calculated as the root mean square of individual standard deviations [19].

According to Eqs. (1) and (2) and when the sum is replaced by integral, Eq. (31) can be rewritten:

$$\bar{\sigma}^2 \cong \frac{1}{N\Delta z}\frac{I_M}{n_{\mathrm{FW}}}\int_0^{N\Delta z}\left\{I_0 + I_A \exp\left[-\left(\frac{z - z_M}{l_c}\right)^2\right] \times \cos\left[\frac{4\pi}{\lambda_0}(z - z_M) + \varphi\right]\right\} \mathrm{d}z. \tag{32}$$

For $l_c > \lambda_0$ (which is always satisfied in white-light interferometry), the contribution of the exponential function to the integral in Eq. (32) can be neglected. Thus, the mean standard deviation of the noise is given by

$$\bar{\sigma} \cong \sqrt{\frac{I_M I_0}{n_{\mathrm{FW}}}}. \tag{33}$$

By inserting the mean standard deviation $\bar{\sigma}$ into Eq. (17), we obtain the lower limit of the measurement uncertainty for the modulated signal with a signal-dependent noise:

$$\delta z = \sigma_{z_M} \geq C\sqrt{2}\sqrt[4]{\frac{2}{\pi}}\sqrt{\frac{I_M}{n_{\mathrm{FW}}}}\frac{\sqrt{I_0}}{I_A}\sqrt{\Delta z l_c}. \tag{34}$$

For the ideal evaluation, Eq. (34) goes over to

$$\delta z \geq \sqrt{2}\sqrt[4]{\frac{2}{\pi}}\sqrt{\frac{I_M}{n_{\mathrm{FW}}}}\frac{\sqrt{I_0}}{I_A}\sqrt{\Delta z l_c}. \tag{35}$$

Because the shot noise imposes a basic limit on the minimal signal-to-noise ratio, the result of Eq. (35) provides a limit of measurement uncertainty on rough surfaces that cannot be gone below.

The result expressed by Eqs. (34) and (35) can be illustrated by an example with typical values used in white-light interferometry on rough surfaces. Let us

consider a white-light interferometry setup shown in Fig. 1 with an LED as a light source and a CCD camera at the output. The used LED has a central wavelength of $\lambda_0 = 850\ nm$ and spectral width of FWHM $= 40\ nm$. The CCD camera is provided with an eight bit AD converter. The full-well capacity of the camera is $n_{\mathrm{FW}} = 100{,}000$, corresponding to the maximal intensity $I_M = 255$ DN. The measured signal has an offset of $I_0 = 100$ DN, and the amplitude of modulation is of $I_A = 80$ DN. The signal is measured with the sampling step of $\Delta z = 0.085\ \mu m$ that corresponds to five steps per period. (Because of Michelson arrangement, the period of modulation is equal to $\lambda_0/2$.) The signal (interferogram) is shown in Fig. 6.

For a light source with $\lambda_0 = 850\ nm$ and FWHM $= 40\ nm$, it holds that [32]

$$l_c \cong \frac{\sqrt{\ln 2}}{\pi}\frac{\lambda_0^2}{\mathrm{FWHM}} = 4.8\ \mu m. \tag{36}$$

Then according to Eq. (35), the lower limit of the measurement uncertainty is equal to $\delta z = 5.1 \times 10^{-3}\ \mu$m for ideal evaluation of the interferogram. In our experiments, we use the evaluation of interferograms with $L = l_c$. Such a setting proved to give satisfactory results. According to Eq. (18), it holds $C \cong 1.16$. The lower limit of the measurement uncertainty is then equal to $\delta z = 5.9 \times 10^{-3}\ \mu$m.

The measurement uncertainty of white-light interferometry on rough surfaces is mainly influenced by the surface roughness. The measurement uncertainty introduced by surface roughness is given by [32,33]

$$\delta z_{\mathrm{rough}} = \frac{1}{\sqrt{2}}\sqrt{\frac{\langle I_{\mathrm{obj}}\rangle}{I_{\mathrm{obj}}}}R_q, \tag{37}$$

where R_q is the root-mean-square roughness of the surface, I_{obj} is the local intensity, and $\langle I_{\mathrm{obj}}\rangle$ is the mean intensity of the speckle pattern. The subscript "obj" emphasizes that intensities I_{obj} and $\langle I_{\mathrm{obj}}\rangle$ are measured when only the object arm of the interferometer is illuminated (the reference beam is shut off to eliminate the influence of interference). The relation between the measurement uncertainty introduced by the shot noise and that introduced by the surface roughness can be illustrated on an example. For a surface with $R_q = 1\ \mu$m and for a speckle with the intensity equal to the mean intensity of the speckle pattern $I_{\mathrm{obj}} = \langle I_{\mathrm{obj}}\rangle$, the measurement uncertainty is equal to $\delta z_{\mathrm{rough}} = 0.71\ \mu$m. On the other hand, the example given below Eq. (35) yields the result $\delta z = 5.9 \times 10^{-3}\ \mu$m.

On usual conditions, the measurement uncertainty introduced by surface roughness is much higher than that introduced by the shot noise. This explains the result described in [10] that the coherence length of the light source has almost no influence on the measurement uncertainty when measured on optically rough surfaces. However, in high-speed applications of white-light interferometry on rough surfaces, high values of l_c and Δz are used [34]. In this case, the measurement uncertainty caused by shot noise can become comparable with that caused by surface roughness. The comparison of the results expressed by Eqs. (35) and (37) indicates for which conditions the measurement uncertainty introduced by surface roughness is dominant.

8. Conclusions

The analysis of the lower limit of measurement uncertainty introduced by the noise has been performed for white-light interferometry on rough surfaces. The measurement uncertainty is directly proportional to the noise-to-signal ratio and to the square root of the product of the sampling step and coherence length of the used light. The measurement uncertainty of white-light interferometry (sensor with modulated signal) is by a factor $\sqrt{2}$ higher than that of a sensor with the signal without modulation.

Additionally, the lower limit of measurement uncertainty introduced by shot noise only has been calculated for white-light interferometry on rough surfaces. The measurement uncertainty is again directly proportional to the noise-to-signal ratio and to the square root of the product of the sampling step and coherence length of the used light. In the case of shot noise, the noise-to-signal ratio depends on the mean intensity of the signal and the full-well capacity of the used camera.

The derived relations can be useful for the estimation of the measurement uncertainty introduced by noise for both white-light interferometry and a sensor with signal without modulation. They enable us to choose the parameters of the experimental arrangement to keep the measurement uncertainty within desired limits. The measurement uncertainty introduced by shot noise provides a limit measurement uncertainty that cannot be gone below (in the framework of classical optics).

We wish to thank Professor Jan Peřina and Professor Lubomír Kubáček for interesting discussions and useful suggestions leading to the preparation of this paper.

This research was supported financially by the Operational Program Research and Development for Innovations—European Social Fund (projects CZ.1.05/2.1.00/03.0058 and CZ.1.07/2.3.00/20.0017).

References

1. G. S. Kino and S. S. C. Chim, "Mirau correlation microscope," Appl. Opt. **29**, 3775–3783 (1990).
2. B. S. Lee and T. C. Strand, "Profilometry with a coherence scanning microscope," Appl. Opt. **29**, 3784–3788 (1990).
3. T. Dresel, G. Haüsler, and H. Venzke, "Three-dimensional sensing of rough surfaces by coherence radar," Appl. Opt. **31**, 919–925 (1992).
4. P. J. Caber, "Interferometric profiler for rough surfaces," Appl. Opt. **32**, 3438–3441 (1993).
5. L. Deck and P. de Groot, "High-speed noncontact profiler based on scanning white-light interferometry," Appl. Opt. **33**, 7334–7338 (1994).

6. K. G. Larkin, "Efficient nonlinear algorithm for envelope detection in white light interferometry," J. Opt. Soc. Am. A **13**, 832–843 (1996).
7. G. Häusler, P. Ettl, M. Schenk, G. Bohn, and I. Laszlo, "Limits of optical range sensors and how to exploit them," in *International Trends in Optics and Photonics ICO IV*, T. Asakura, ed., Springer Series in Optical Sciences (Springer-Verlag, 1999), Vol. 74, pp. 328–342.
8. G. Häusler, "Speckle and Coherence," in *Encyclopedia of Modern Optics*, B. D. Guenther, ed. (Elsevier, Academic, 2005), pp. 114–123.
9. P. Ettl, B. Schmidt, M. Schenk, I. Laszlo, and G. Häusler, "Roughness parameters and surface deformation measured by coherence radar," Proc. SPIE **3407**, 133–140 (1998).
10. Z. Saraç, R. Gross, C. Richter, B. Wiesner, and G. Haüsler, "Optimization of white light interferometry on rough surfaces based on error analysis," Optik **115**, 351–357 (2004).
11. G. Haüsler, "Three-dimensional sensors—potential and limitations," in *Handbook of Computer Vision and Applications*, B. Jähne, H. Haussecker, and P. Geissler, eds. (Academic, 1999), pp. 485–506.
12. M. Hering, K. Körner, and B. Jähne, "Correlated speckle noise in white-light interferometry: theoretical analysis of measurement uncertainty," Appl. Opt. **48**, 525–538 (2009).
13. M. Fleischer, R. Windecker, and H. J. Tiziani, "Theoretical limits of scanning white-light interferometry signal evaluation algorithms," Appl. Opt. **40**, 2815–2820 (2001).
14. M. Fox, *Quantum Optics* (Oxford University, 2006).
15. B. Jähne, "Continuous and digital signals," in *Handbook of Computer Vision and Applications*, B. Jähne, H. Haussecker, and P. Geissler, eds. (Academic, 1999), pp. 9–34.
16. T. Seiffert, "Verfahren zur schnellen Signalaufnahme in der Weisslichtinterferometrie," Ph.D. dissertation (University Erlangen-Nuremberg, 2007).
17. H.-E. Albrecht, M. Borys, N. Damaschke, and C. Tropea, *Laser Doppler and Phase Doppler Measurement Techniques* (Springer-Verlag, 2003).
18. M. Born and E. Wolf, *Principles of Optics* (Cambridge University, 2003).
19. K. F. Riley, M. P. Hobson, and S. J. Bence, *Mathematical Methods for Physics and Engineering* (Cambridge University, 2004).
20. L. Kubáček, *Foundations of Estimation Theory* (Elsevier, 1988).
21. J. W. Goodman, "Statistical properties of laser speckle patterns," in *Laser Speckle and Related Phenomena*, J. C. Dainty, ed. (Springer-Verlag, 1984), pp. 9–75.
22. I. S. Gradshteyn and I. M. Ryzhik, *Table of Integrals, Series, and Products* (Academic, 2000).
23. M. Fleischer, R. Windecker, and H. J. Tiziani, "Fast algorithms for data reduction in modern optical three-dimensional profile measurement systems with MMX technology," Appl. Opt. **39**, 1290–1297 (2000).
24. A. K. Ruprecht, T. F. Wiesendanger, and H. J. Tiziani, "Signal evaluation for high-speed confocal measurements," Appl. Opt. **41**, 7410–7415 (2002).
25. T. Wilson, *Confocal Microscopy* (Academic, 1990).
26. W. Gong, K. Si, and C. J. R. Sheppard, "Optimization of axial resolution in a confocal microscope with D-shaped apertures," Appl. Opt. **48**, 3998–4002 (2009).
27. S. K. Nayar and Y. Nakagawa, "Shape from focus," IEEE Trans. Pattern Anal. Mach. Intell. **16**, 824–831 (1994).
28. Y. An, G. Kang, I.-J. Kim, H.-S. Chung, and J. Park, "Shape from focus through Laplacian using 3D window," in *Proceedings of IEEE Second International Conference on Future Generation Communication and Networking* (IEEE, 2008), pp. 46–50.
29. R. Onodera, H. Watanabe, and Y. Ishii, "Interferometric phase-measurement using a one-dimensional discrete Hilbert transform," Opt. Rev. **12**, 29–36 (2005).
30. M. Kendall, A. Stuart, and J. K. Ord, *The Advanced Theory of Statistics* (Charles Griffin, 1983).
31. J. Peřina, *Quantum Statistics of Linear and Nonlinear Optical Phenomena* (Kluwer Academic, 1991).
32. P. Pavliček and O. Hýbl, "White-light interferometry on rough surfaces—measurement uncertainty caused by surface roughness," Appl. Opt. **47**, 2941–2949 (2008).
33. T. Dresel, "Grundlagen und Grenzen der 3D-Datengewinnung mit dem Kohärenzradar," Master's thesis (University Erlangen-Nuremberg, 1991).
34. R. Gross, O. Hýbl, B. Knapp, and G. Häusler, "Ultrafast 4-Megapixel white-light interferometry," in *DGaO Proceedings* (German Society for Applied Optics, 2009), http://www.dgao-proceedings.de/download/110/110_p17.pdf.